Hindawi
Journal of Nanomaterials
Volume 2022, Article ID 5957125, 10 pages
https://doi.org/10.1155/2022/5957125

Research Article

Influence of Cu-Doping Concentration on the Structural and Optical Properties of SnO_2 Nanoparticles by Coprecipitation Route

Abebe G. Habte,[1] **Fekadu Gashaw Hone**,[2] **and F. B. Dejene**[3]

[1]*Physics Department, Hawassa University, P.O. Box 5, Hawassa, Ethiopia*
[2]*Physics Department, Addis Ababa University, P.O. Box 1176, Addis Ababa, Ethiopia*
[3]*Department of Chemical and Physical Sciences, Walter Sisulu University, Private Bag X1, Code 5117, Mthatha, South Africa*

Correspondence should be addressed to Fekadu Gashaw Hone; fekeye@gmail.com

Received 18 May 2022; Revised 22 September 2022; Accepted 5 October 2022; Published 11 November 2022

Academic Editor: Marinella Striccoli

Tin dioxide (SnO_2) nanoparticles doped with varying concentrations of copper were synthesized and characterized using various techniques. The X-ray diffraction analysis revealed that all doped and undoped SnO_2 samples had a rutile-type tetragonal structure. The average crystalline size of the doped samples estimated using Scherrer's formula and the Williamson–Hall plot decreased as dopant concentration increased. Images from scanning electron microscopy revealed spherical grains in the samples. The transmission electron microscope was used to examine the particle nature, and nearly spherical particles were discovered. The energy-dispersive X-ray spectroscopy analyses confirmed that the synthesized nanoparticles were nearly stoichiometrically composed of the expected elements copper, oxygen, and tin. The bandgap energy of doped and undoped SnO_2 nanoparticles was determined using UV–visible diffuse reflectance spectra, and it was found to decrease as Cu^{2+} ion concentration increased. The photoluminescence study at the excitation wavelength of 300 nm revealed defect-oriented emissions between 350 and 500 nm. All the obtained results showed that the physical properties of SnO_2 can be easily engineered through Cu doping for various optoelectronic applications using a low-cost coprecipitation method.

1. Introduction

Tin dioxide (SnO_2) is an important n-type, wide-bandgap semiconductor with excellent optical, electrochemical, and electrical properties [1]. SnO_2 with a tetragonal structure has an energy bandgap of about 3.6 eV at room temperature [2]. It has a wide range of applications, including lithium-ion storage batteries [3, 4], transparent conducting electrodes [5, 6], gas sensors [7, 8], optoelectronic devices [9, 10], photovoltaic cells, photo detectors, and so on. To obtain the required properties for specific applications, the morphology and size of SnO_2 nanoparticles must be controlled during synthesis [11–13]. Doping SnO_2 with specific metal ions is an efficient method for changing the optical, electrical, and magnetic properties of SnO_2 nanostructures [7]. Several doping elements, such as Cu, Zn, Ni, La, and Co, have been used to tune the properties of SnO_2 nanomaterials [14–17]. The practical performance of SnO_2 is determined by crystallinity, surface morphology, and crystal size, all of which are determined by the synthesis method. To prepare SnO_2 nanostructures, various synthesis techniques such as solid-state reaction [6], sol–gel [18–20], coprecipitation [10], hydrothermal [21], and microwave assisted [22] have been developed. Among these methods, coprecipitation produces stoichiometric and homogeneous nanoparticles at a low cost. Nanocrystalline SnO_2 properties are highly dependent on preparation methods and dopant materials. Dopant elements can change the microstructure and defect chemistry of SnO_2, resulting in changes in physical and chemical properties [23]. Many studies have been published on the influence of Cu doping on the physical properties of SnO_2 nanomaterials. Mishra et al. [24] studied the role of Cu doping on the formaldehyde sensing of SnO_2 nanoparticles using stannic tetrachloride hydrated ($SnCl_4{\cdot}5H_2O$). Thermal evaporation method was employed to grow Cu-doped SnO_2 nanowires for H_2S gas sensors by Kumar et al. [25]. Lavanya et al. [26]

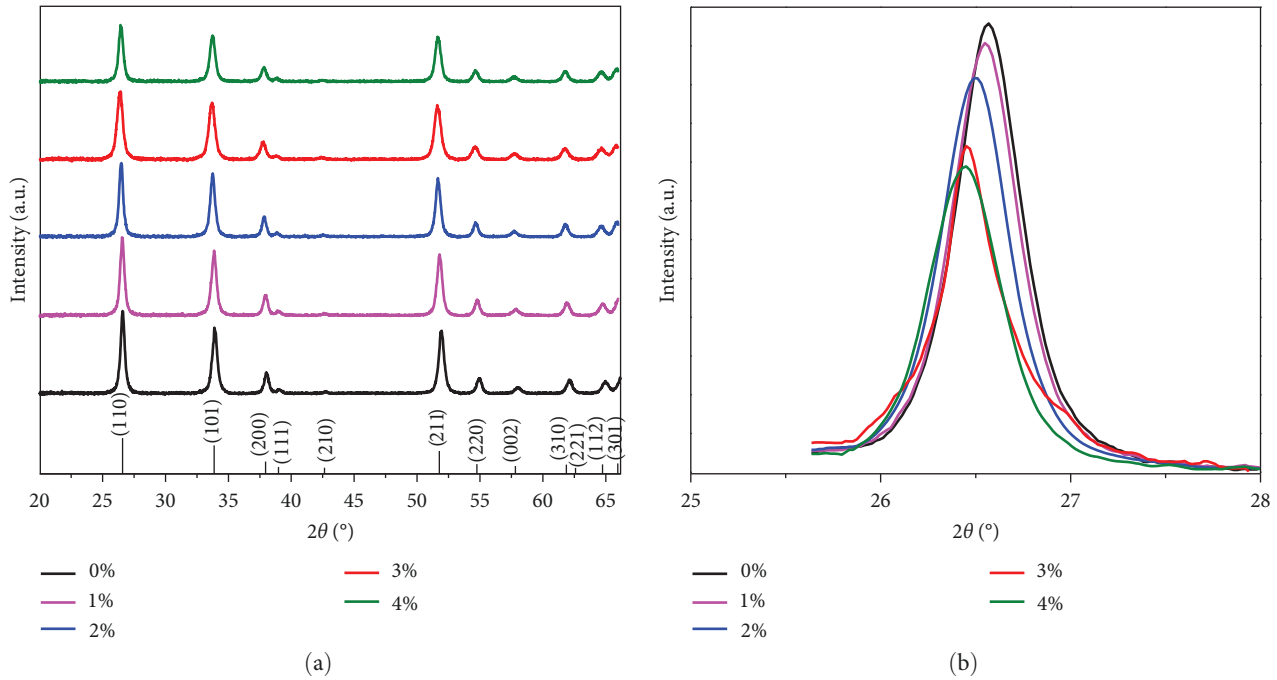

FIGURE 1: (a) The XRD pattern of pure and Cu-doped SnO_2 nanoparticles; (b) magnified view of the shifting of (110) plane for pure and Cu-doped SnO_2.

reported the synthesis of Cu-doped SnO_2 nanoparticles by microwave irradiation method for the precise determination of folic acid. Chetri et al. [27] investigated the structural and optical properties of Cu-doped SnO_2 nanostructures using experiments and correlated the observations with density functional theory results. Thermal evaporation and condensation method was employed to synthesize Cu-doped SnO_2 nanobelts by Li et al. [28] and the temperature dependance photoluminescence (PL) properties of the nanobelts and samples annealed in oxygen were studied. The main challenge in the addition of dopants is the synthesis of nanoparticles without secondary phases. In light of this, we chose cost-effective coprecipitation method, which allows the chemicals to be mixed at the atomic level, avoiding the formation of undetectable impurity phases. From the existing report, copper metal ions would be a perfect material to be used as a dopant. In this study, we reported the synthesis of pure and Cu-doped SnO_2 via a simple co-precipitation method. The effects of Cu-doping on essential structural, optical, and morphological properties have been studied systematically. The obtained results revealed that Cu doping has a significant influence on the physical properties of the host nanomaterial.

2. Experiment

2.1. Sample Preparation. The synthesis of SnO_2 nanoparticles was started by the dissolving of 0.132 mol of tin dichloride dihydrate ($SnCl_2{\cdot}2H_2O$) in deionized water and allowed it to stirrer for 5 min. Copper (II) acetate monohydrate Cu $(CH_3COO)_2{\cdot}H_2O$ was taken as the source of dopant. The dopant solution of the required amount (1%, 2%, 3%, and 4%) was slowly added drop by drop to the previous precursor solution with continuing magnetic stirring. The pH of the solution was kept around 9.8 by adding aqueous ammonia (NH_3, 25%) solution drop wise. It was then heated at 50°C for 2 hr with vigorous stirring. The final solution was washed repeatedly with deionized water and ethanol to get chlorine ion-free SnO_2 nanoparticles. The resulting product was kept for 24 hr at room temperature and then dried for 1 hr at 70°C. Finally, smaller and homogeneous powder particles were obtained. The prepared samples were annealed at 600°C for 2 hr to get crystallized nanoparticles.

2.2. Characterization. The structures of the prepared Cu-doped and pure SnO_2 nanoparticles were measured by using a powder X-ray diffraction (XRD), model Bruker D8 advance, Germany equipped with CuKα irradiation ($\lambda = 1.5406$ Å) in the range of 2θ from 20° to 66°. The UV–Vis spectra of the samples were recorded in diffuse reflectance mode using a Perkin Elmer Lambda 950 UV–Vis spectrometer in the range of 250–800 nm. The room temperature PL measurements were carried out by an F-7000 FL spectrophotometer. The surface morphology and elemental composition of the samples were studied using a high-resolution JEOL JSM-7800F scanning electron microscope equipped with energy-dispersive X-ray (EDX) analysis. Transmission electron microscope (TEM) measurements were done using a Philips CM 100 microscope.

3. Results and Discussion

3.1. Structure Analyses. The XRD spectrum of undoped and Cu-doped SnO_2 samples is displayed in Figure 1(a). The diffraction pattern corresponds to the rutile type phase of SnO_2 with tetragonal structure (JCPDS 41-1445) showing a preferred orientation along the (110) plane. All the observed

Table 1: The structural parameters and optical bandgap of pure and Cu-doped SnO_2 nanoparticles.

Doping level	Scherrer's method		W–H method		Lattice constants (Å)		Unit cell volume $(Å)^3$	Energy bandgap (eV)
	D (nm)	Density of dislocation ($\times 10^{15}$ lines/m^2)	D (nm)	Strain ($\times 10^{-3}$)	$a = b$	c		
0%	19.01	2.76	24.53	0.148	4.740	3.188	71.626	3.74
1%	18.23	3.00	23.56	0.70	4.744	3.193	71.860	3.69
2%	17.54	3.23	23.32	1.06	4.751	3.196	72.140	3.65
3%	14.87	4.52	16.56	1.22	4.761	3.196	72.444	3.61
4%	13.79	5.25	15.38	1.31	4.761	3.197	72.466	3.54

diffraction peaks were sharp and strong, which showed that the synthesized samples were fully crystallized and polycrystalline in nature. The addition of copper did not affect the preferred orientation along the (110) plane and crystal structure. No diffraction peaks due to copper or copper oxide were visible in the pattern, which revealed that the produced nanostructure had a tetragonal phase structure of SnO_2. The Cu-doped samples indicate that SnO_2 is still in the rutile phase, suggesting a substitutional doping of Cu at Sn-site [26]. The diffraction peak intensity decreased with an increase in Cu^{2+} ion concentrations, which revealed that the doping induces defects in the nanostructure, hindering the growth of the SnO_2 crystal grains [29]. The lattice parameters ($a = b$, and c) for the tetragonal phase structure were calculated from the XRD peaks using Equation (1):

$$\frac{1}{d_{hkl}^2} = \frac{h^2 + k^2}{a^2} + \frac{l^2}{c^2}, \quad (1)$$

where the plane spacing (d_{hkl}) was calculated by Bragg's law, $n\lambda = 2d_{hkl}\sin(\theta_{hkl})$.

The diffraction peaks shifted toward the lower angle as the copper concentration increased. This indicated that Cu^{2+} ions have been incorporated into the crystal lattice of SnO_2, thereby developing lattice strain within the host crystal lattice [30, 31]. Figure 1(b) displays the (110) peak shift of SnO_2 prepared at different dopant concentrations. The diffraction peaks were affected by lattice strain and crystallite size, which increased the peak width and shifted the 2θ peak position [30]. The shifting of the peaks toward the lower angle increased the d-spacing, indicating the expansion of lattice parameters as well as the unit cell volume of the Cu-doped SnO_2 crystal. The average lattice constants determined from the diffraction planes were found to be $a = b = 4.752$ Å, $c = 3.194$ Å, and their ratio $c/a = 0.672$ (Table 1) which matches with the reference file data values $a = 4.738$ Å, $c = 3.187$ Å, and $c/a = 0.672$. The small difference comes from the microstructural tensile strain due to the incorporation of more Cu^{2+} ions which have a larger ionic radius (0.073 nm) than the tin ions (0.069 nm) [27]. The c/a parameter has also been found to show a good match with the value for the ideally close-packed tetragonal structure (0.672). The lattice parameters variation with Cu-doping concentration is presented in Figure 2(a).

The increase of the full-width at half-maximum (FWHM) with Cu^{2+} ion concentration is an indication of the decrease of crystallite size in the doped SnO_2 samples [32, 33] (Figure 2(b)). The average crystallite size was calculated by Scherrer's formula and Williamson–Hall (W–H) plot. The three highest diffraction peaks, (110), (101), and (211) were used to estimate the crystallite size (D) by Scherrer's formula (Equation (2)) [34]:

$$D_s = \frac{k\lambda}{\beta_s \cos\theta}, \quad (2)$$

where λ is X-ray wavelength ($\lambda = 1.5406$ Å); k is the shape factor (0.9); β is full width at half maximum of the diffraction peak in radians and θ is Bragg diffraction angle in radians.

The lattice strain (ε) and crystallite size were calculated from W–H plot, $\beta\cos\theta$ versus $4\sin\theta$ (Figure 3(a)) [35]. We obtained the strain and crystal size from the slope of the linear-fitted data and the intercepts of the curve, respectively [36]. The reason for the development of the strain could be due to the presence of Cu^{2+} ion dopant. The estimated strain increased with the addition of the dopant concentration (Table 1). The difference in the values of the crystal size determined from the Scherrer formula and W–H plot can be ascribed to the fact that W–H plot considers the broadening caused by the effects of tensile strain. The results from both methods indicated that as the doping concentration increased from 1% to 4%, the crystal size decreased. A similar trend of change in crystal size was reported by different literatures [37, 38] for Cu-doped SnO_2 nanoparticles. This decrease in crystal size of SnO_2 as the Cu-doping level increases suggesting that the growth was suppressed due to doping of Cu^{2+} ion into Sn site. This can be attributed to the incorporation of Cu^{2+} ion in the host lattice to create more nucleation sites which would increase the lattice strain by slowing down the growth of the crystals [37, 39]. The density of dislocation ($\delta = 1/D^2$) [35, 40], where D is the crystallite size from Scherrer's formula, caused by the microstructural strain and other defects seen to increase as Cu-doping increased in the host lattice (Figure 3(b)).

3.2. SEM, EDX, and TEM Analyses. The study of the surface morphology of Cu-doped and undoped SnO_2 nanoparticle has been carried out using scanning electron microscopy

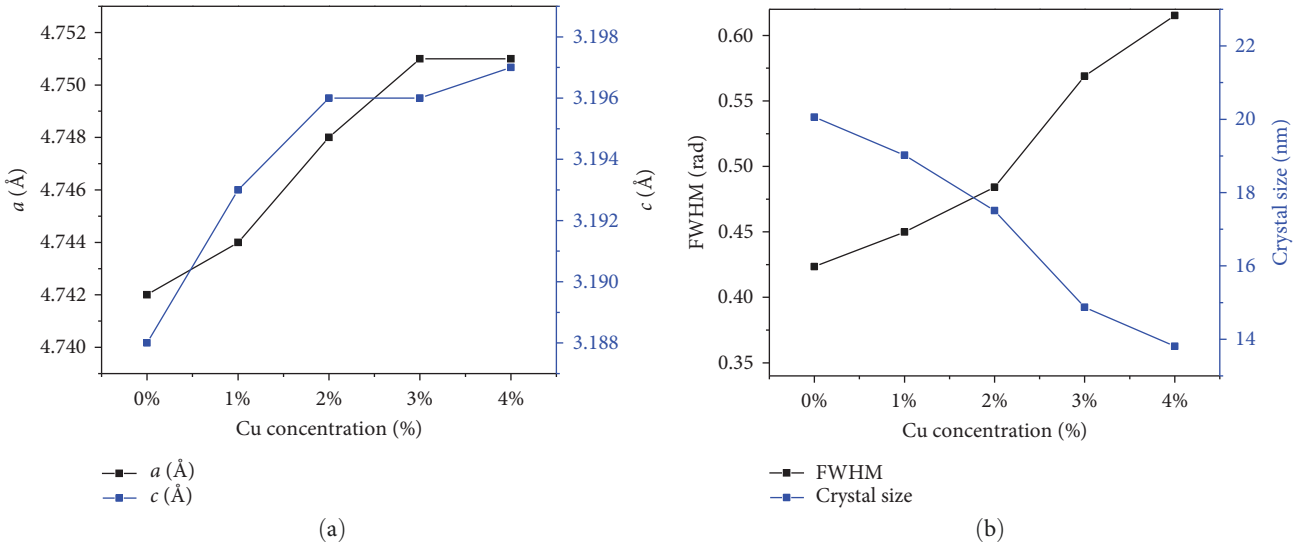

Figure 2: (a) Variation of lattice parameters a and c with Cu-doping concentration; (b) crystal size and FWHM analysis graph of SnO_2 with Cu-doping concentration.

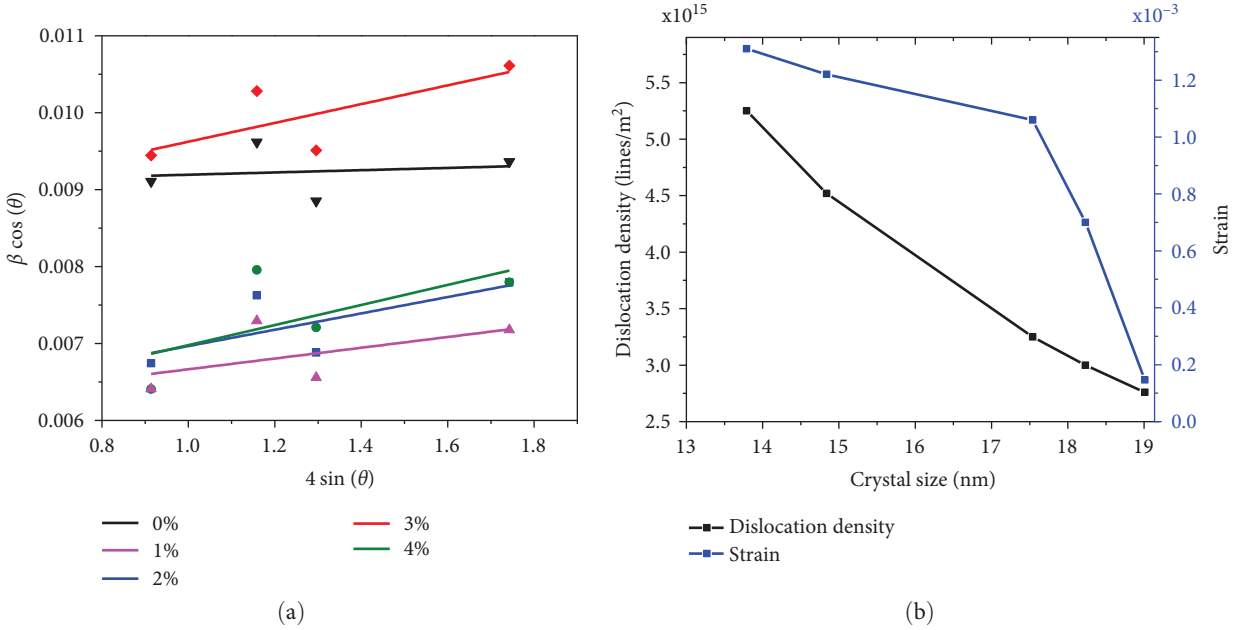

Figure 3: (a) Williamson–Hall plots of undoped and Cu-doped SnO_2 nanoparticle; (b) variation of strain and dislocation density with crystal size.

(SEM) coupled with EDX spectroscopy. The SEM images with 60 KX magnification are presented in Figure 4(a)–4(e). A closer inspection of the images showed that the Cu-doped and undoped samples contained spherical-shaped grains and the morphology of SnO_2 nanoparticles changed with increasing Cu-doping concentration. Depending on the dopant contents, the particles were agglomerated with different sizes. This could be an indication for the formation of larger grain sizes through clustering of the primary particles. The rate of nucleation and growth processes influences the size distribution of the grain and the extent of agglomeration [41]. Figure 4(f)–4(h) illustrates the TEM images of the synthesized samples with 0%, 2%, and 4% of copper doping, respectively. They showed nearly spherical-shaped particles. The particle size distributions for Cu-doped SnO_2 nanoparticles were estimated from TEM images. It can be seen from the images that the particles are nonuniform in size and have an average grain size of 33.60, 29.42, and 26.71 nm for the samples with 0%, 2% and 4% Cu-doping, respectively.

The EDX study was also carried out for looking at the elemental composition of the synthesized samples. The EDX analysis was done at different places in the same sample which confirmed the fairly uniform composition of the nanocrystals. The EDX spectra and their percentage composition of 0%, 1%,

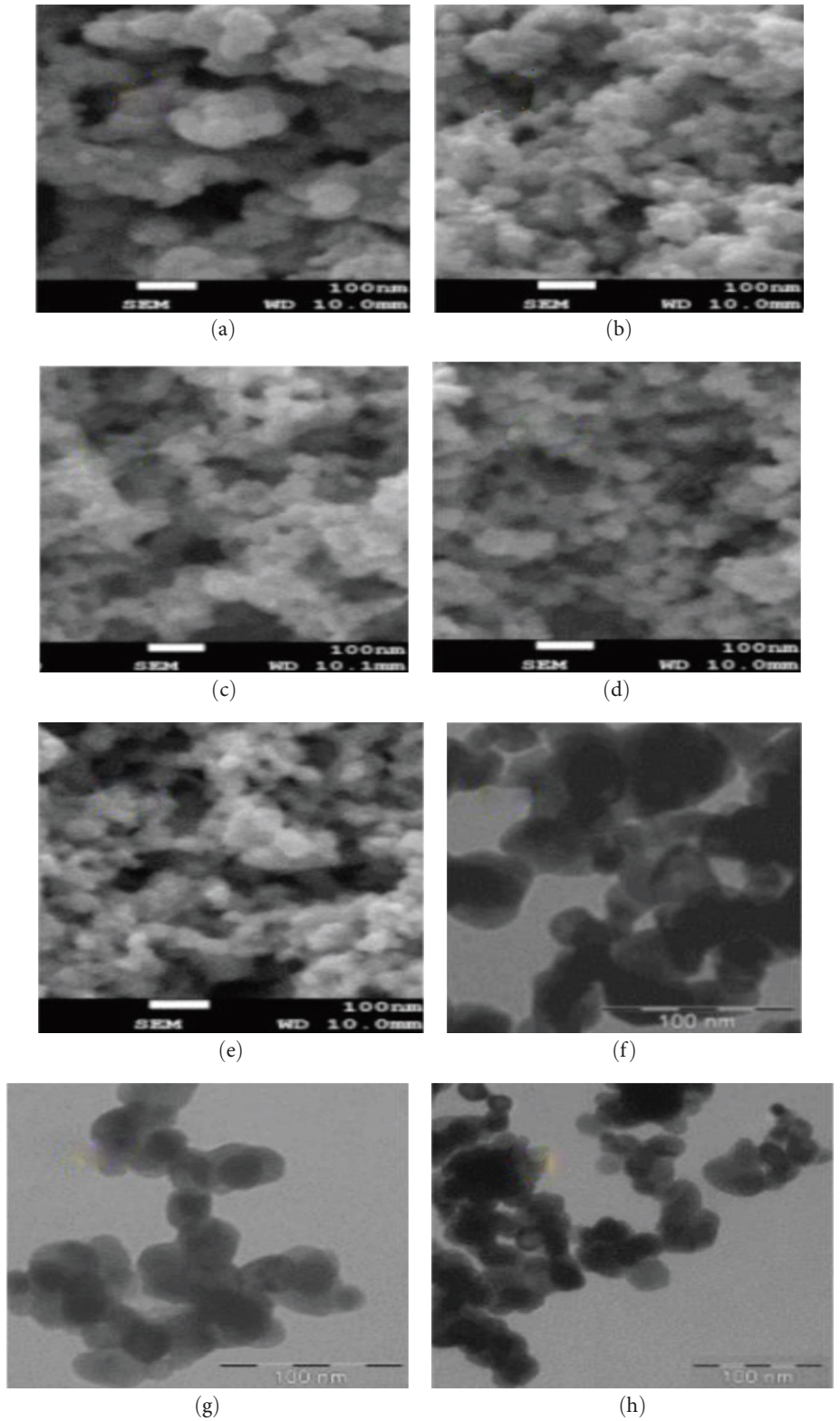

Figure 4: SEM images of (a) pure SnO_2; (b) 1% Cu-doped; (c) 2% Cu-doped; (d) 3% Cu-doped; and (e) 4% Cu-doped SnO_2. TEM micrographs of (f) pure SnO_2; (g) 2% Cu-doped SnO_2; (h) 4% Cu-doped SnO_2.

3%, and 4% Cu-doped samples are shown in Figure 5(a)–5(d). The spectra for the doped samples confirm the incorporation of Cu^{2+} ions into SnO_2 lattice. The atomic percentages composition is close to the stoichiometric ratio for all samples.

3.3. Optical Properties Analyses. The UV–Visible diffuse reflectance spectra of SnO_2 doped with copper were recorded in the 250–800 nm wavelength range. It provides useful information about the optical bandgap of the prepared Cu-doped

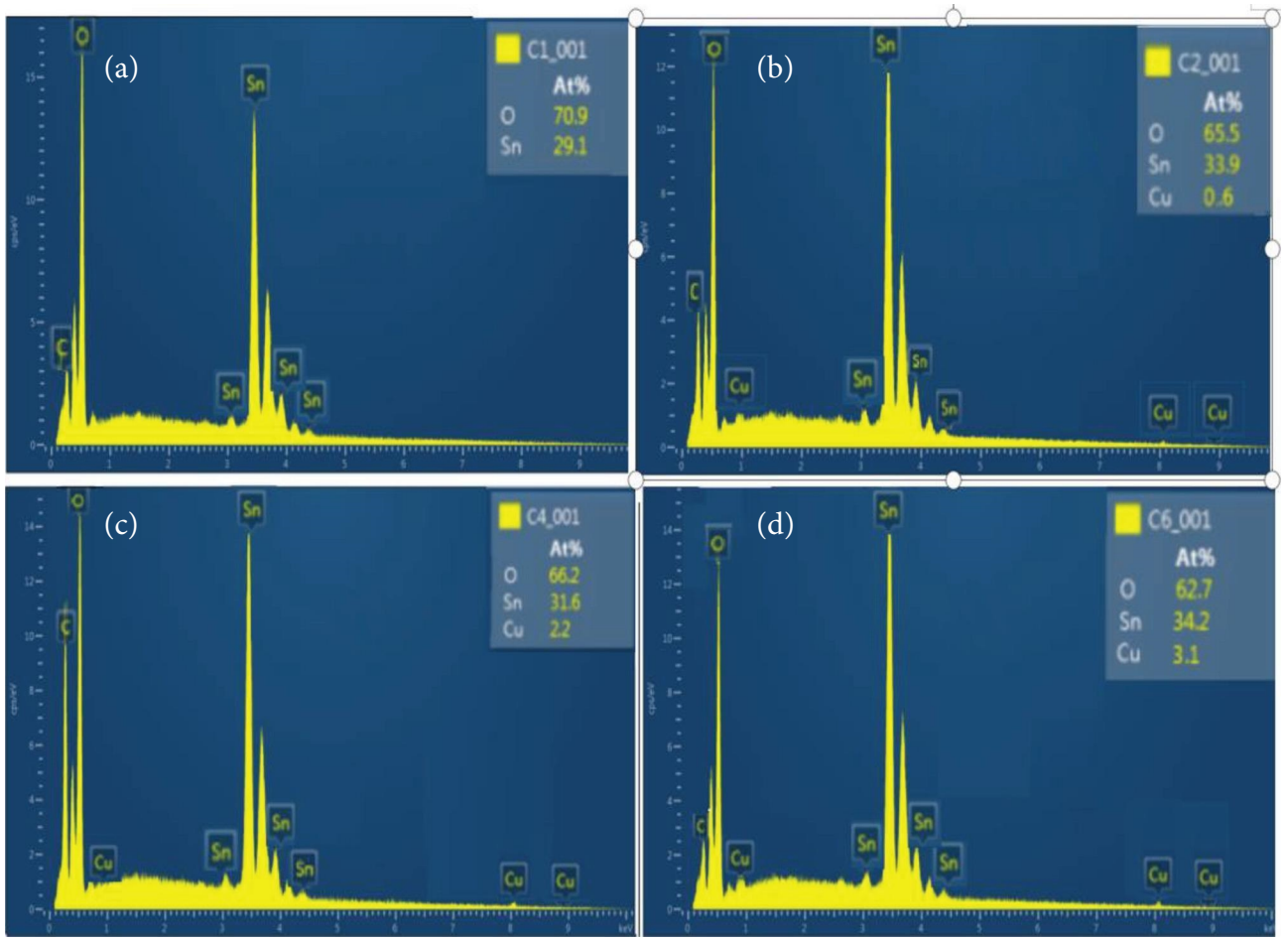

Figure 5: EDX spectra of (a) pure SnO_2; (b) 1% Cu-doped; (c) 3% Cu-doped; (d) 4% Cu-doped SnO_2 nanoparticle.

and undoped samples. The percentage diffuse reflectance of the produced nanostructures is presented in Figure 6(a). The samples have high reflectance spectrum in the visible region but showed small reflectance in the UV region. This might be due to the transfer of charge from the valence to the conduction band of SnO_2 nanostructures [42]. Tauc's relation (Equation (3)) was used to calculate the bandgap (E_g) of the prepared samples:

$$\alpha h\nu = A\left(h\nu - E_g\right)^n, \tag{3}$$

where A is a constant, $h\nu$ is the photon energy, α is the absorption coefficient and n is equal to 1/2 for the direct allowed transition. To determine the value of the optical bandgap of Cu-doped SnO_2, the reflectance values were converted to absorbance by applying the Kubelka–Munk transformation function (Equation (4)):

$$F(R) = \frac{(1-R)^2}{2R}, \tag{4}$$

where R is the percentage reflectance and $F(R)$ is the Kubelka–Munk function which is proportional to the absorption coefficient (α).

In Figure 6(b), the absorption spectrum exhibits only one absorption edge with no visible shoulder on the lower energy side, indicating the absence of any secondary phase-related absorption edges. To estimate the bandgap, we extrapolate the linear portion of the $(F(R)h\nu)^2$ versus $h\nu$ curve to zero, where $h\nu$ is the photon energy [43]. From Figure 6(b), the bandgap energy obtained from the curve was around 3.74 eV for undoped. The magnitude of bandgap was decreasing from 3.69 to 3.54 eV as Cu-dopant concentration increased from 1% to 4% (Table 1). A similar narrowing in the bandgap was reported in the literature for the doping of SnO_2 with copper [25, 37]. We find that the absorption edge is red shifted with increasing Cu^{2+} ion content in SnO_2 lattice. Presence of dopant introduces impurity band levels into the bandgap of tin oxide. The narrowing bandgap energy is possibly due to the existence of copper impurities in the SnO_2 structure, which induce the formation of new recombination centers with lower emission energy [17]. Thus, with a greater amount of copper ions, the transition of electrons occurs from the filled valence band to the new recombination centers instead of the transition of electrons from the filled valence band to the empty conduction band which usually occurs [44].

3.4. Photoluminescence Analyses. The PL technique has been widely used to examine the defects and to understand the fate of photogenerated electrons and holes in semiconductors [45].

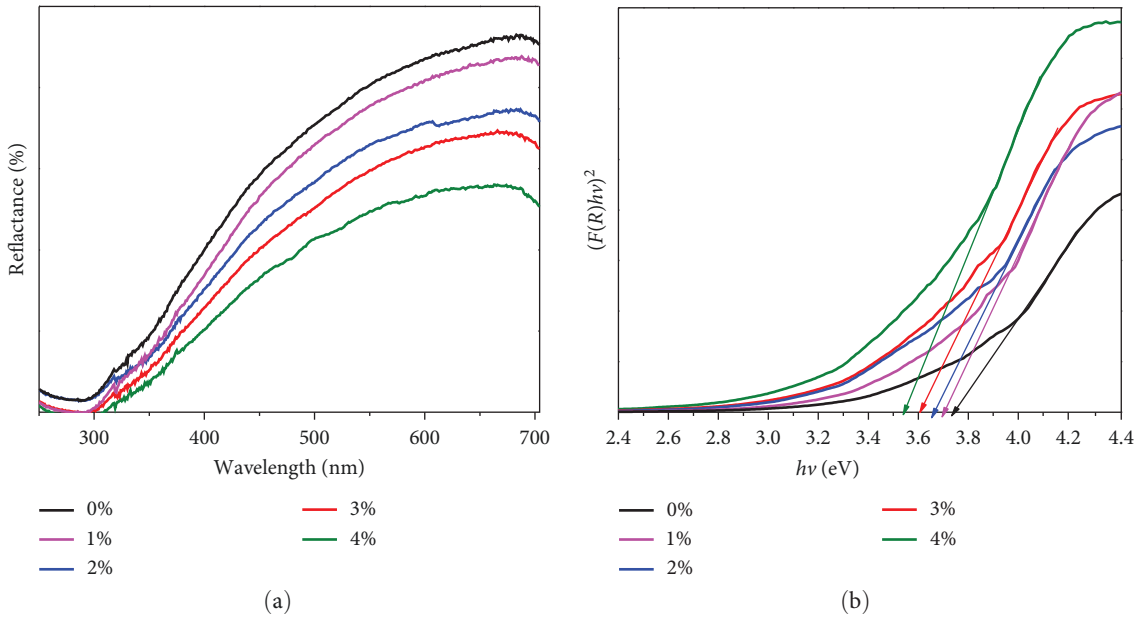

FIGURE 6: (a) UV–Vis diffuse reflectance spectra versus wavelength; (b) Tauc's plot of $(F(R)hv)^2$ versus photon energy.

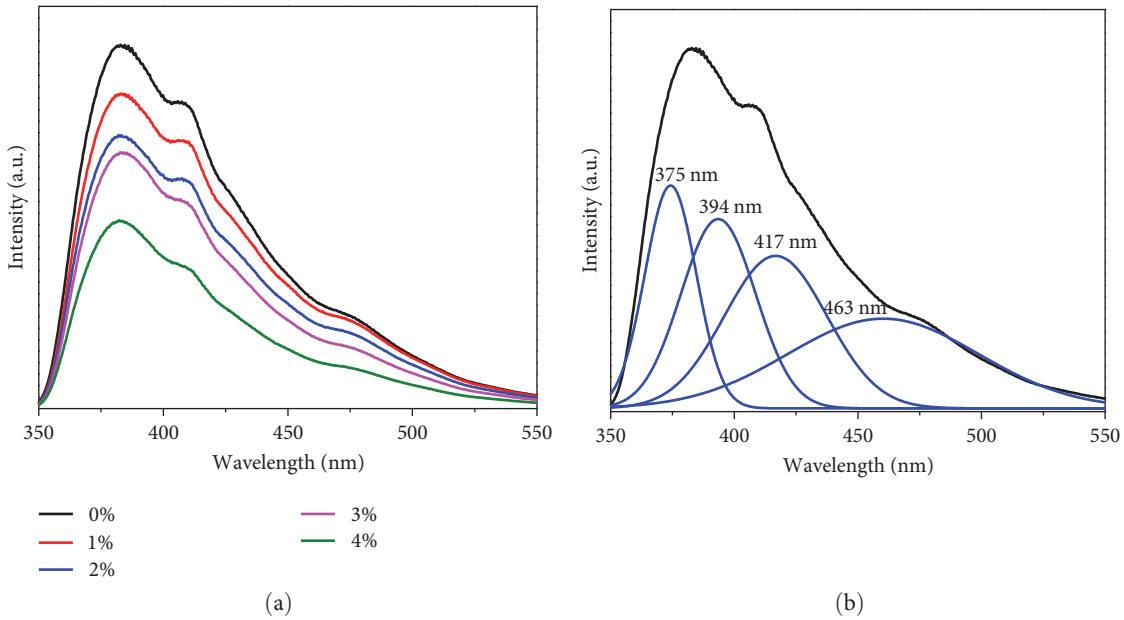

FIGURE 7: (a, b) PL emission spectra of undoped and Cu-doped SnO_2 nanoparticles excited at 280 nm.

Usually, metal-doped SnO_2 nanostructures display defect emissions. These defects might include oxygen vacancies and the luminescence center formed by tin interstitial or the presence of dangling bonds in SnO_2 nanoparticles [46]. The oxygen vacancies are the main defects, which form the donor levels in SnO_2 nanostructures [47]. The defects are mainly located on the surface of the nanostructures and could form a series of energy levels within the bandgap of SnO_2 by trapping electrons from the valence band. The room temperature PL spectrum was recorded at an excitation wavelength of 300 nm as shown in Figure 7(a). The broad spectrum measured from the undoped sample was deconvoluted by to four components centered at 375, 395, 417, and 463 nm using Gaussian fitting, as shown in Figure 7(b). These emission energies are much lower than the energy bandgap of SnO_2 calculated from the diffuse reflectance spectra; therefore, the electron from the conduction band was not directly recombined to a hole in the valance band; instead, they are assigned to the electron transition, mediated by defect levels in the bandgap.

The UV emission around 375 nm may be attributed to the transition of electrons mediated by oxygen vacancies [1, 48]. Oxygen vacancies are the most common defects which form donor levels inside the bandgap [49]. The UV emission was due to the transition of electrons from the donor level to the valence band. The peak around 395 nm can be attributed to

the electron transition mediated by defect levels in the band. The defects are mainly located on the surface of the nanostructures and could form a series of energy levels within the bandgap of SnO_2 nanomaterials by trapping electrons from the valence band [50]. The peak around 417 nm is attributed to the tin interstitial present in the nanocrystals which forms a significant amount of trapped in the bandgap of SnO_2 nanocrystals [48]. It is reported that the SnO_2 nanostructures can exhibit emission in the visible region because of the presence of different defect energy levels inside the SnO_2 bandgap [10, 51]. The visible emission around 463 nm may be attributed to the formation of luminescent centers formed by defects [52, 53].

It can also be seen that the PL intensity of the undoped SnO_2 is higher than that in the spectra of Cu-doped samples, indicating that copper doping can inhibit the excited electron and hole recombination. An intensity reduction was observed for the emission peaks with an increase in Cu-doping concentration [37]. This could be attributed to a concentration quenching effect characterized by the energy exchange between a pair of Cu^{2+} ions [24].

4. Conclusion

Nanocrystalline Cu-doped SnO_2 was successfully synthesized via a simple coprecipitation technique at variable Cu-doping concentrations. The XRD analysis showed a tetragonal structure for all Cu-doped and undoped SnO_2 samples. The average crystallite size decreased with the increasing of Cu-dopant concentration. A shift in the (110) SnO_2 plane confirmed the incorporation of dopants in the crystal lattice. The doping of copper atoms, with greater ionic radius than Sn atoms in the host, created a tensile strain in the lattice and caused expanded lattice parameters of the produced nanoparticles. The SEM micrographs showed spherically shaped particles. The TEM images confirmed that the prepared undoped and Cu-doped SnO_2 were in nano size. The optical studies revealed that Cu doping in the SnO_2 lattice reduced the bandgap energy from 3.74 to 3.54 eV. The noticed red shift in the bandgap was due to the incorporation of Cu^{2+} ions in the host lattice which created additional energy levels inside the bandgap. The PL spectra exhibited UV and visible emissions between 350 and 500 nm due to defects such as oxygen vacancies and the luminescence center formed by tin interstitial or the presence of dangling bonds in SnO_2 nanoparticles.

Data Availability

The data used to support the findings of this study are available from the corresponding author upon request.

Conflicts of Interest

The authors declare that they have no conflicts of interest.

References

[1] B. Venugopal, B. Nandan, A. Ayyachamy et al., "Influence of manganese ions in the band gap of tin oxide nanoparticles: structure, microstructure and optical studies," *RSC Advances*, vol. 4, no. 12, pp. 6141–6150, 2014.

[2] E. Thamarai Selvi and S. Meenakshi Sundar, "Effect of Mn doping on structural, optical and magnetic properties of SnO_2 nanoparticles by solvothermal processing," *Journal of Materials Science: Materials in Electronics*, vol. 28, no. 20, pp. 15021–15032, 2017.

[3] H. Song, X. Li, Y. Cui et al., "Controllable lithium storage performance of tin oxide anodes with various particle sizes," *International Journal of Hydrogen Energy*, vol. 40, pp. 14314–14321, 2015.

[4] C. Mrabet, A. Boukhachem, M. Amlouk, and T. Manoubi, "Improvement of the optoelectronic properties of tin oxide transparent conductive thin films through lanthanum doping," *Journal of Alloys and Compounds*, vol. 666, pp. 392–405, 2016.

[5] D. Haridas and V. Gupta, "Enhanced response characteristics of SnO_2 thin film based sensors loaded with Pd clusters for methane detection," *Sensors and Actuators B: Chemical*, vol. 166-167, pp. 156–164, 2012.

[6] E. T. H. Tan, G. W. Ho, A. S. W. Wong, S. Kawi, and A. T. S. Wee, "Gas sensing properties of tin oxide nanostructures synthesized via a solid-state reaction method," *Nanotechnology*, vol. 19, no. 25, Article ID 255706, 2008.

[7] J. Wang, C. Lu, X. Liu, Y. Wang, Z. Zhu, and D. Meng, "Synthesis of tin oxide (SnO & SnO_2) micro/nanostructures with novel distribution characteristic and superior photocatalytic performance," *Materials & Design*, vol. 115, pp. 103–111, 2017.

[8] R. Yousefi, "Effects of Sn atoms on formation of ZnO nanorings," *CrystEngComm*, vol. 17, pp. 2698–2704, 2015.

[9] M. P. Subramaniam, G. Arunachalam, R. Kandasamy, P. Veluswamy, and I. Hiroya, "Effect of pH and annealing temperature on the properties of tin oxide nanoparticles prepared by sol–gel method," *Journal of Materials Science: Materials in Electronics*, vol. 29, pp. 658–666, 2018.

[10] G. Singh and R. C. Singh, "Synthesis and characterization of Gd-doped SnO_2 nanostructures and their enhanced gas sensing properties," *Ceramics International*, vol. 43, no. 2, pp. 2350–2360, 2017.

[11] H. Kaur, H. S. Bhatti, and K. Singh, "Effect of organic solvents on photocatalytic activity of PEG-capped SnO_2 nanoparticles," *Journal of Materials Science: Materials in Electronics*, vol. 29, pp. 2026–2034, 2018.

[12] V. Kumar, K. Singh, A. Kumar et al., "Effect of solvent on crystallographic, morphological and optical properties of SnO_2 nanoparticles," *Materials Research Bulletin*, vol. 85, pp. 202–208, 2017.

[13] C. A. Ibarguen, A. Mosquera, R. Parra, M. S. Castro, and J. E. Rodríguez-Páez, "Synthesis of SnO_2 nanoparticles through the controlled precipitation route," *Materials Chemistry and Physics*, vol. 101, no. 2–3, pp. 433–440, 2007.

[14] K. Sakthiraj and K. Balachandrakumar, "Influence of Ti addition on the room temperature ferromagnetism of tin oxide (SnO_2) nanocrystal," *Journal of Magnetism and Magnetic Materials*, vol. 395, pp. 205–212, 2015.

[15] Z. Lin, N. Li, Z. Chen, and P. Fu, "The effect of Ni doping concentration on the gas sensing properties of Ni doped SnO_2," *Sensors and Actuators B: Chemical*, vol. 239, pp. 501–510, 2017.

[16] X. Kou, C. Wang, M. Ding et al., "Synthesis of Co-doped SnO_2 nanofibers and their enhanced gas-sensing properties," *Sensors and Actuators B: Chemical*, vol. 236, pp. 425–432, 2016.

[17] S. Lekshmy and K. Joy, "Structural and optoelectronic properties of indium doped SnO_2 thin films deposited by sol gel technique," *Journal of Materials Science: Materials in Electronics*, vol. 25, pp. 1664–1672, 2014.

[18] M. Aziz, S. S. Abbas, W. R. W. Baharom, and W. Z. W. Mahmud, "Structure of SnO_2 nanoparticles by sol–gel method," *Materials Letters*, vol. 74, pp. 62–64, 2012.

[19] V. Senthilkumar, P. Vickraman, and R. Ravikumar, "Synthesis of fluorine doped tin oxide nanoparticles by sol–gel technique and their characterization," *Journal of Sol-Gel Science and Technology*, vol. 53, pp. 316–321, 2010.

[20] A.-M. Ungureanu, O. Oprea, B. S. Vasile, C. Andronescu, G. Voicu, and I. Jitaru, "Temperature effect over structure and photochemical properties of nanostructured SnO_2 powders," *Central European Journal of Chemistry*, vol. 12, no. 9, pp. 909–917, 2014.

[21] M. A. M. Akhir, K. Mohamed, H. L. Lee, and S. A. Rezan, "Synthesis of tin oxide nanostructures using hydrothermal method and optimization of its crystal size by using statistical design of experiment," *Procedia Chemistry*, vol. 19, pp. 993–998, 2016.

[22] M. Akram, A. T. Saleh, W. A. W. Ibrahim, A. S. Awan, and R. Hussain, "Continuous microwave flow synthesis (CMFS) of nano-sized tin oxide: effect of precursor concentration," *Ceramics International*, vol. 42, no. 7, pp. 8613–8619, 2016.

[23] V. Kumar, K. Singh, J. Sharma, A. Kumar, A. Vij, and A. Thakur, "Zn-doped SnO_2 nanostructures: structural, morphological and spectroscopic properties," *Journal of Materials Science: Materials in Electronics*, vol. 28, pp. 18849–18856, 2017.

[24] R. K. Mishra, A. Kushwaha, and P. P. Sahay, "Influence of Cu doping on the structural, photoluminescence and formaldehyde sensing properties of SnO_2 nanoparticles," *RSC Advances*, vol. 4, no. 8, pp. 3904–3912, 2014.

[25] V. Kumar, S. Sen, K. P. Muthe, N. K. Gaur, S. K. Gupta, and J. V. Yakhmi, "Copper doped SnO_2 nanowires as highly sensitive H_2S gas sensor," *Sensors and Actuators B: Chemical*, vol. 138, no. 2, pp. 587–590, 2009.

[26] N. Lavanya, S. Radhakrishnan, N. Sudhan et al., "Fabrication of folic acid sensor based on the Cu doped SnO_2 nanoparticles modified glassy carbon electrode," *Nanotechnology*, vol. 25, no. 29, Article ID 295501, 2014.

[27] P. Chetri, B. Saikia, and A. Choudhury, "Structural and optical properties of Cu doped SnO_2 nanoparticles: an experimental and density functional study," *Journal of Applied Physics*, vol. 113, Article ID 233514, 2013.

[28] L. J. Li, K. Yu, H. B. Mao, and Z. Q. Zhu, "Photoluminescence and field-emission properties of Cu-doped SnO_2 nanobelts," *Applied Physics A*, vol. 99, no. 4, pp. 865–869, 2010.

[29] N. Lavanya, C. Sekar, E. Fazio, F. Neri, S. G. Leonardi, and G. Neri, "Development of a selective hydrogen leak sensor based on chemically doped SnO_2 for automotive applications," *International Journal of Hydrogen Energy*, vol. 42, no. 15, pp. 10645–10655, 2017.

[30] R. K. Mishra and P. P. Sahay, "Zn-doped and undoped SnO_2 nanoparticles: a comparative structural, optical and LPG sensing properties study," *Materials Research Bulletin*, vol. 47, no. 12, pp. 4112–4118, 2012.

[31] N. M. Shaalan, D. Hamad, A. Aljaafari, A. Y. Abdel-Latief, and M. A. Abdel-Rahim, "Preparation and characterization of developed $Cu_xSn_{1-x}O_2$ nanocomposite and its promising methane gas sensing properties," *Sensors*, vol. 19, no. 10, Article ID 2257, 2019.

[32] S. Gautam, A. Thakur, A. Vij et al., "X-ray spectroscopy study of $Zn_xSn_{1-x}O_2$ nanorods synthesized by hydrothermal technique," *Thin Solid Films*, vol. 546, pp. 250–254, 2013.

[33] N. Shanmugam, T. Sathya, G. Viruthagiri, C. Kalyanasundaram, R. Gobi, and S. Ragupathy, "Photocatalytic degradation of brilliant green using undoped and Zn doped SnO_2 nanoparticles under sunlight irradiation," *Applied Surface Science*, vol. 360, Part A, pp. 283–290, 2016.

[34] A. G. Habte, F. G. Hone, and F. B. Dejene, "The influence of malonic acid on the structural, morphological and optical properties of CdSe thin films prepared by chemical bath deposition method," *Inorganic Chemistry Communications*, vol. 103, pp. 107–112, 2019.

[35] E. T. Seid, F. B. Dejene, Z. N. Urgessa, and J. R. Botha, "Refluxed sol–gel synthesized ZnO nanopowder with variable zinc precursor concentrations," *Applied Physics A*, vol. 124, Article ID 738, 2018.

[36] M. K. Hussen, F. B. Dejene, and G. G. Gonfa, "Effect of citric acid on material properties of $ZnGa_2O_4$:Cr^{3+} nanopowder prepared by sol-gel method," *Applied Physics A*, vol. 124, Article ID 390, 2018.

[37] S. Sagadevan, Z. Z. Chowdhury, M. R. B. Johan et al., "Cu-doped SnO_2 nanoparticles: synthesis and properties," *Journal of Nanoscience and Nanotechnology*, vol. 19, no. 11, pp. 7139–7148, 2019.

[38] S. Benzitouni, M. Zaabat, A. Khial et al., "High sensitivity of porous Cu-doped SnO_2 thin films to methanol," *Advances in Nanoparticles*, vol. 5, no. 2, pp. 140–148, 2016.

[39] S. A. Saleh, A. A. Ibrahim, and S. H. Mohamed, "Structural and optical properties of nanostructured Fe-doped SnO_2," *Acta Physica Polonica A*, vol. 129, no. 6, pp. 1220–1225, 2016.

[40] S. Thanikaikarasan, K. Sundaram, T. Mahalingam, S. Velumani, and J.-K. Rhee, "Electrodeposition and characterization of Fe doped CdSe thin films from aqueous solution," *Materials Science and Engineering: B*, vol. 174, no. 1–3, pp. 242–248, 2010.

[41] V. Kumar, K. Singh, K. Singh, S. Kumari, A. Kumar, and A. Thakur, "Effect of solvent on the synthesis of SnO_2 nanoparticles," *AIP Conference Proceedings*, vol. 1728, Article ID 020532, 2016.

[42] S. Mugundan, B. Rajamannan, G. Viruthagiri, N. Shanmugam, R. Gobi, and P. Praveen, "Synthesis and characterization of undoped and cobalt-doped TiO_2 nanoparticles via sol–gel technique," *Applied Nanoscience*, vol. 5, pp. 449–456, 2015.

[43] F. Dejene, A. Ali, H. Swart et al., "Optical properties of ZnO nanoparticles synthesized by varying the sodium hydroxide to zinc acetate molar ratios using a sol–gel process," *Central European Journal of Physics*, vol. 9, no. 5, pp. 1321–1326, 2011.

[44] P. Baraneedharan, S. Imran Hussain, V. P. Dinesh, C. Siva, P. Biji, and M. Sivakumar, "Lattice doped Zn–SnO_2 nanospheres: a systematic exploration of dopant ion effects on structural, optical, and enhanced gas sensing properties," *Applied Surface Science*, vol. 357, Part B, pp. 1511–1521, 2015.

[45] R. Yousefi, M. Moradi, G. H. Bordbar, and M. A. M. Teridi, "Role of non-stoichiometric defects in optical properties of metal-selenide nanostructures," *Journal of Luminescence*, vol. 223, Article ID 117211, 2020.

[46] N. Salah, S. Habib, A. Azam, M. S. Ansari, and W. M. Al-Shawafi, "Formation of Mn-doped SnO_2 nanoparticles via the microwave technique: structural, optical and electrical properties," *Nanomaterials and Nanotechnology*, vol. 6, 2016.

[47] V. Kumar, V. Kumar, S. Som et al., "The role of surface and deep-level defects on the emission of tin oxide quantum dots," *Nanotechnology*, vol. 25, Article ID 135701, 2014.

[48] G. Zhang, S. Zhang, L. Yang, Z. Zou, D. Zeng, and C. Xie, "La_2O_3-sensitized SnO_2 nanocrystalline porous film gas sensors and sensing mechanism toward formaldehyde," *Sensors and Actuators B: Chemical*, vol. 188, pp. 137–146, 2013.

[49] P. S. Shewale, K. Ung Sim, Y.-B. Kim, J. H. Kim, A. V. Moholkar, and M. D. Uplane, "Structural and photoluminescence characterization of SnO_2: F thin films deposited by advanced spray pyrolysis technique at low substrate temperature," *Journal of Luminescence*, vol. 139, pp. 113–118, 2013.

[50] V. Kalimuthu and S. Rath, "UV photoluminescence from nanocrystalline tin oxide synthesized by a one-step hydrothermal method," *Materials Letters*, vol. 157, pp. 11–14, 2015.

[51] L. V. Thong, N. Loan, and N. Van Hieu, "Comparative study of gas sensor performance of SnO_2 nanowires and their hierarchical nanostructures," *Sensors and Actuators B: Chemical*, vol. 150, no. 1, pp. 112–119, 2010.

[52] P. Rajeshwaran and A. Sivarajan, "Influence of Mn doping on structural, optical and acetone gas sensing properties of SnO_2 nanoparticles by a novel microwave technique," *Journal of Materials Science: Materials in Electronics*, vol. 26, pp. 539–546, 2015.

[53] S. Das, S. Kar, and S. Chaudhuri, "Optical properties of SnO_2 nanoparticles and nanorods synthesized by solvothermal process," *Journal of Applied Physics*, vol. 99, Article ID 114303, 2006.